

ARTICLE



APE1 inhibition enhances ferroptotic cell death and contributes to hepatocellular carcinoma therapy

Yu Du ^{1,2}, Yu Zhou^{1,2}, Xinyu Yan¹, Feiyan Pan ¹, Lingfeng He ¹, Zhigang Guo ¹✉ and Zhigang Hu ¹✉

© The Author(s), under exclusive licence to ADMC Associazione Differenziamento e Morte Cellulare 2024

Ferroptosis, a regulated form of cell death triggered by iron-dependent lipid peroxidation, has emerged as a promising therapeutic strategy for cancer treatment, particularly in hepatocellular carcinoma (HCC). However, the mechanisms underlying the regulation of ferroptosis in HCC remain to be unclear. In this study, we have identified a novel regulatory pathway of ferroptosis involving the inhibition of Apurinic/apyrimidinic endonuclease 1 (APE1), a key enzyme with dual functions in DNA repair and redox regulation. Our findings demonstrate that inhibition of APE1 leads to the accumulation of lipid peroxidation and enhances ferroptosis in HCC. At the molecular level, the inhibition of APE1 enhances ferroptosis which relies on the redox activity of APE1 through the regulation of the NRF2/SLC7A11/GPX4 axis. We have identified that both genetic and chemical inhibition of APE1 increases AKT oxidation, resulting in an impairment of AKT phosphorylation and activation, which leads to the dephosphorylation and activation of GSK3 β , facilitating the subsequent ubiquitin-proteasome-dependent degradation of NRF2. Consequently, the downregulation of NRF2 suppresses SLC7A11 and GPX4 expression, triggering ferroptosis in HCC cells and providing a potential therapeutic approach for ferroptosis-based therapy in HCC. Overall, our study uncovers a novel role and mechanism of APE1 in the regulation of ferroptosis and highlights the potential of targeting APE1 as a promising therapeutic strategy for HCC and other cancers.

Cell Death & Differentiation; <https://doi.org/10.1038/s41418-024-01270-0>

INTRODUCTION

Hepatocellular carcinoma (HCC) is one of the leading causes of cancer-related deaths. According to the Global Cancer Report 2020, HCC is now the sixth most prevalent malignancy and the third leading cause of cancer-related death worldwide, with increasing incidence and mortality. Although treatment strategies for HCC are gradually becoming more intensive, including surgery, immunotherapy, targeted therapy, or combination approaches, the effectiveness of these treatments and the availability of effective drugs, as well as their duration of efficacy, remain limited. Consequently, the overall survival rate of HCC patients continues to be constrained [1]. Hence, there is an urgent need to better understand the underlying mechanisms of liver cancer pathogenesis and identify effective therapeutic targets.

Currently, emerging studies have implied the involvement of ferroptosis in cancer progression and therapy, particularly in HCC. Ferroptosis is an iron-dependent regulated necrosis mediated by lipid peroxidation, which represents a novel pathway of cell death that is distinctly different from apoptosis, necrosis, and autophagy at the level of morphological, biochemical, and genetic [2]. It is considered a natural tumor suppression mechanism and plays a significant role in the anti-cancer effects of many cancer therapies including radiotherapy, immunotherapy, and certain chemotherapy approaches [3–5]. Current studies indicate that ferroptosis is mainly induced by the peroxidation of phospholipids (PLs) that contain polyunsaturated fatty acids (PUFAs) [6]. Ferroptosis can be modulated by several crucial factors, including solute carrier family 7 member 11 (SLC7A11), the key transporter of cystine, and

glutathione peroxidase 4 (GPX4) [7, 8]. SLC7A11 imports extracellular cystine into the cell, which is subsequently converted to glutathione (GSH) [7]. In turn, GPX4 utilizes GSH to reduce lipid hydroperoxides, thus inhibiting ferroptosis [8]. Correspondingly, the genetic or pharmacological inactivation of GPX4 or SLC7A11 has been shown to induce ferroptosis [9]. Many studies have found that activation of the nuclear factor E2-related factor 2 (NRF2) increases the expression of SLC7A11 and GPX4 to inhibit the development of ferroptosis in cells [10]. Recently, many studies have implicated ferroptosis in the development of HCC and have explored its potential as a novel therapeutic approach and prognostic indicator for HCC [10]. It was found that cytokine signaling 2 (SOCS2) specifically accelerates the ubiquitinated degradation of SLC7A11, thereby enhancing ferroptosis in HCC and sensitivity to radiotherapy [11]. Furthermore, depletion of glutathione s-transferase zeta 1 (GSTZ1) has been found to activate the NRF2 pathway, leading to an increase in GPX4 expression and inhibiting sorafenib-induced ferroptosis in HCC [12]. Therefore, targeting Ferroptosis may be a new promising therapeutic strategy for HCC.

Apurinic/apyrimidinic endonuclease 1 (APE1), also known as reduction-oxidation factor-1 (REF1), is a multifunctional enzyme with a molecular weight of 36.5 kDa [13]. Initially identified as a DNA repair enzyme, APE1 plays a central role in the repair of DNA damage caused by endogenous oxidative stress and alkylating agents through the well-conserved base excision repair (BER) pathway [14, 15]. Later on, APE1 was independently

¹Jiangsu Key Laboratory for Molecular and Medical Biotechnology, College of Life Sciences, Nanjing Normal University, 1 WenYuan Road, Nanjing 210023, China. ²These authors contributed equally: Yu Du, Yu Zhou. ✉email: guo@njnu.edu.cn; huzg_2000@126.com

Received: 3 August 2023 Revised: 11 February 2024 Accepted: 12 February 2024

Published online: 28 February 2024

recognized as a multifunctional protein involved not only in DNA damage repair (DDR) but also in regulating gene expression through its redox activity [16]. Many stress-responsive transcription factors including nuclear factor- κ B (NF- κ B) [17], hypoxia-inducible factor-1 α (HIF-1 α) [18], activator protein-1 (AP-1) [19], p53 [20], and others have been reported to be activated by APE1-dependent redox activation. Just like many other key DNA damage repair genes, APE1 is widely involved in the progression of various cancers, such as HCC [21]. Of note, high levels of APE1 have been associated with resistance to chemotherapy in HCC and poor clinical outcome [22]. Targeting DNA repair genes for cancer therapy has been applied as adjuvant therapy in chemotherapy and immunotherapy in several kinds of cancers [23–25]. Most DDR inhibition strategies are dependent on inducing cell apoptosis. Our previous study identified that APE1 inhibition induced several kinds of cell death, such as apoptosis, necroptosis, and pyroptosis [26]. In addition, two recent studies found that APE1 participates in ferroptosis in gastric cancer (GC) cells, and the sustained oxidative stress during ferroptosis upregulates the expression of APE1 and increases the resistance to ferroptosis [27, 28]. In this study, we found a novel role and mechanism of APE1 in regulating ferroptosis in HCC by regulating the NRF2/SLC7A11/GPX4 axis. Inhibition of APE1 sensitized HCC cells to ferroptosis inducers and significantly promoted ferroptosis. Moreover, APE1-mediated ferroptosis was associated with its redox activity, but not with its DNA repair activity involved in BER. Using tumor xenografts in nude mice, we further demonstrated that inhibition of APE1 impeded HCC progression and contributed to ferroptosis-based HCC therapy in vivo. Overall, our study suggests that APE1 is a novel suppressor of ferroptosis, and targeting the APE1/NRF2 axis may be an attractive strategy for the treatment of HCC and other kinds of cancers.

MATERIALS AND METHODS

Antibodies and reagents

The antibodies to APE1 (10203-1-AP), NRF2 (16396-1-AP), SLC7A11 (26864-1-AP), GPX4 (67763-1-Ig), p53 (60283-2-Ig), p-GSK3 β (67558-1-Ig), AKT (10176-2-AP), p-AKT (Ser473) (80455-1-RR) and ubiquitin (10201-2-AP) were obtained from Proteintech. The antibody to Tubulin (AM1031a) was obtained from Abcepta. The antibody to γ -H2AX (80312S) was obtained from Cell Signaling Technology. The antibody to HIF-1 α (340462) was obtained from ZENBIO. The antibodies to GSK3 β (A11731), HRP Goat Anti-Rabbit IgG (AS014), and HRP Goat Anti-Mouse IgG (AS003) were obtained from ABclonal. CRT0044876, Erastin, and Ferrostatin-1 were purchased from Topscience (Shanghai, China). E3330, RSL-3, Z-VAD-FMK, Necrostatin 2, Chloroquine, and AR-A014418 were obtained from GlpBio (Montclair, CA, USA). 4-acetamido-4'-maleimidylstilbene-2,2'-disulfonic acid (AMS) was obtained from Thermo Fisher Scientific (Waltham, MA, USA). Corn oil was obtained from Shanghai Yuanye Bio-Technology Co., Ltd (Shanghai, China). Ipatasertib was obtained from Selleck (Houston, TX, USA).

Plasmid construction

APE1-knockdown (KD) lentivirus was constructed and purified by the **Vigenebio (Shangdong, China)**. The NRF2 overexpression plasmid, siAKT, and siGSK3 β were purchased from **Vigenebio (Shangdong, China)**. For the knockdown of NRF2 the silencing plasmids containing shRNA sequences were constructed based on psilencer3.0-H1. The cDNAs of wild type APE1 (APE1-WT), APE1 DNA damage repair mutant (APE1-H309N), and APE1 redox mutant (APE1-C65A) were cloned into pcDNA6/V5 HisA vector to construct overexpression plasmids. The shRNA, overexpression, siRNA, and mutant primer sequences are listed in Supplementary Table S1. All plasmids were verified by sequencing.

Cell culture and the development of stable cell lines

Human hepatoma cells HepG2 and Huh7 were purchased from the Cell Bank of the Chinese Academy (Shanghai, China). All cells were authenticated by STR profiling and tested for mycoplasma contamination. HepG2 cells were cultured in MEM (KGM41500) supplemented with 10% FBS (BC-SE-FBS07) and 1% penicillin/streptomycin. Huh7 cells were

cultured in DMEM (KGM12800) supplemented with 10% FBS (BC-SE-FBS07) and 1% penicillin/streptomycin. All cell lines were maintained in a humidified atmosphere containing 5% CO₂ at 37 °C and tested for mycoplasma before the commencement of experiments. For APE1-KD HepG2 and Huh7 stable cells, the cells were infected with specific lentivirus vectors for 48 h and then selected with puromycin for two weeks.

ROS and lipid peroxidation assay

Cells were seeded in triplicate in 6-well plates 24 h before treatment, and pretreated with or without drugs for 24 h. Cells in each well were then incubated with fresh medium containing 4 μ M H2DCFDA (MCE, HY-D0940) for ROS measurements or 5 μ M BODIPY 581/591 C11 dye (GlpBio, GC40165) at 37 °C for 30 min. After trypsinizing the cells into a cell suspension, the cells were washed with PBS by centrifugation. ROS and lipid peroxidation levels were analyzed by flow cytometry using a flow cytometer (BIOSINO, ZS-AE7S).

qRT-PCR

Total RNA was extracted using TRIzol reagent (Invitrogen, 15596026CN), and cDNA was synthesized with SuperScript II Reverse Transcriptase (Vazyme, R222-01). The SYBR Green Master Mix Kit (Vazyme, Q341-02) was used for the relative quantification of RNA levels according to the manufacturer's instructions. The CT values were normalized to that of β -actin, and the relative mRNA expression levels of genes were calculated using the 2^{- $\Delta\Delta$ Ct} method. Each sample was analyzed in triplicate. The primers used are listed in Supplementary Table S2.

Western blotting

The cells were washed with PBS three times and lysed in RIPA buffer. The proteins were separated using 10% SDS-PAGE and transferred onto PVDF membranes (Roche, 52130500, Basel, Switzerland). In addition, after blocking in PBS with 5% skim milk for 1.5 h, the membranes were incubated with the corresponding primary antibodies overnight at 4 °C. After washing the membranes three times for 5 min each time with PBST, incubating the secondary antibody for 1 h at room temperature, and then washing the membrane three times with PBST. The chemiluminescence solution was prepared according to the instructions and added to the PVDF membrane in drops. The images were scanned by the Tanon 4500 Imaging System (Tanon, Shanghai, China) and quantified with ImageJ (National Institutes of Health). All original western blots are available in the Supplementary Material.

Determination of redox states

Cell lysates were treated with trichloroacetic acid at a final concentration of 7.5% for 10 min on ice to denature and precipitate proteins and to avoid any subsequent redox reactions. The protein precipitate was collected by centrifugation at 12,000 \times g for 10 min at 4 °C, washed twice with ice-cold acetone, and then dissolved in a buffer containing 50 mM Tris-HCl (pH 7.4), 1% SDS, and 15 mM AMS and incubated for 1 h away from light. Proteins were separated by SDS-PAGE, followed by western blot analysis.

Immunoprecipitation and ubiquitination assays

Cell samples were lysed using Pierce IP Lysis Buffer (25 mM Tris-HCl, pH 7.4, 150 mM NaCl, 1% NP-40, and 5% glycerol; Pierce Biotechnology) supplemented with Halt™ Protease Inhibitor Cocktail. Cell debris was removed by centrifugation at 10,000 g for 10 minutes and the supernatant was incubated with anti-NRF2 antibody at 4 °C overnight with slow rotation. Thirty microliters of A/G-Sepharose was added to each tube and tubes were incubated for 2 h at 4 °C. Precipitates were collected by gentle centrifugation and then washed three times with pre-cooled phosphate-buffered saline. Proteins were eluted with SDS sample buffer and subjected to SDS-PAGE, and proteins were transferred onto PVDF membranes (Millipore). An antibody against ubiquitin was used to measure NRF2 ubiquitination.

Cell viability assay

For viability assays, cells were seeded in 96-well plates and treated with drugs for an appropriate time on the next day. Then, the medium with drugs was removed and replaced with a fresh medium containing 10% Cell Counting Kit-8 (CCK8) reagent (APExBio, K1018). The plate was incubated for 1.5 h at 37 °C and measured the absorbance was at 450 nm using a microplate reader (TECAN infinite F200 PRO).

Determination of redox states

The redox states of proteins were assessed by modifying free thiol with AMS [29]. Briefly, cell lysates or proteins were treated with trichloroacetic acid at a final concentration of 7.5% to denature and precipitate the proteins, thereby preventing any subsequent redox reactions. The protein precipitates were collected through centrifugation at $12,000 \times g$ for 10 min at 4 °C, followed by two washes with acetone. Subsequently, the protein precipitates were dissolved in a buffer containing 50 mM Tris-HCl (pH 7.4), 1% SDS, and 15 mM AMS. Proteins were then detected by Western Blotting as described above.

Transmission electron microscopy analysis

Cells treated with different treatment drugs were collected and fixed in a solution containing 2.5% glutaraldehyde for 24 h. They were then fixed in 1% osmium tetroxide for 2 h. The samples were then dehydrated through an ethanol gradient and subsequently embedded in Spurr's resin. After staining the sections, the ultrastructure of the cells was observed under the transmission electron microscope.

Immunofluorescence analysis

The cells were grown on cover slips in 12-well plates, fixed with 4% paraformaldehyde for 10 min, permeabilized with 0.1% Triton X-100 (Solarbio, T8200, Beijing, China) for 10 min, and blocked with 3% BSA (SunShineBio, B0012-100, Shanghai, China) at room temperature for 1 h. The cells were immunostained with primary antibodies against various proteins overnight at 4 °C. Next, the cells were washed with PBS three times and then stained with the Alexa Fluor 594 or Alexa Fluor 488 conjugated secondary antibodies at room temperature for 2 h. After washing, the cells were stained with DAPI (Bioworld, AC15221, Nanjing, China) at 37 °C for 10 min. Further, after being washed three times with PBS, the coverslips were mounted using an antifading mounting medium (Solarbio, S2100, Beijing, China). The cells were visualized by a fluorescence microscope (Nikon, 801 10-1500X), and the images were captured with a charge-coupled device camera.

Immunohistochemical staining (IHC)

The obtained tissues were fixed using 4% paraformaldehyde, after which the tissues were embedded in paraffin and sectioned. After dewaxing of tissue sections, antigen repair was performed using citrate buffer at a concentration of 10 mM, pH 6.0 at 100 °C. Sections were washed using PBS and the tissue was circled using an immunohistochemical pen to create a hydrophobic isolation zone. The sections were closed using 3% BSA for 1 h. Overnight incubation was performed using a primary antibody, and after washing, incubation was performed for 30 min at room temperature using a secondary antibody. The sections were then stained using 3, 3'-diaminobenzidine (DAB) and counterstained with hematoxylin. The sections were observed and photographed under a light microscope and analyzed using ImageJ software.

Tumor xenografts

All animal experiments were performed according to the procedures approved by the Laboratory Animal Care Committee at Nanjing Normal University (Permit number IACUC-20201202) and followed the National Institutes of Health guide for the care and use of Laboratory animals. Five weeks old female nude mice were purchased from GemPharmatech Co., Ltd (Nanjing, China), and were maintained under specific pathogen-free conditions for subcutaneous inoculation. 1×10^7 APE1 knockdown and control Huh7 cancer cells were implanted subcutaneously into the right dorsal flanks of C57BL/6 mice (five mice per group), respectively. When the tumors reached a certain size, the mice were randomly divided into four groups (five mice per group) and treated with DMSO, and Erastin (10 mg/kg) by intraperitoneal injection every two days until the end of treatment. Tumor volume was measured every four days (tumor volume was calculated by the following formula: tumor volume = length \times width² \times 1/2) until the endpoint.

Bioinformatic analysis

The expression of APE1, SLC7A11, and GPX4 in hepatocellular carcinoma and normal samples analyzed by the Gene Expression Profiling Interactive Analysis (GEPIA) online database (<http://gepia.cancer-pku.cn/index.html>), as well as generating survival curves for HCC patients with high and low APE1 expression and analyzing the correlation of APE1 with SLC7A11 and GPX4 genes. The mRNA expression data were downloaded from the Gene

Expression Omnibus (GEO) database and processed using standard methods to analyze the expression of APE1.

Statistical analysis

Statistical analysis was performed with GraphPad Prism 8.0. Statistical significance was determined using a two-tailed Student's *t* test or analysis of variance in the case of comparisons among multiple groups. $p < 0.05$ was considered statistically significant.

RESULTS

Inhibition of APE1 promotes ferroptosis in HCC cells

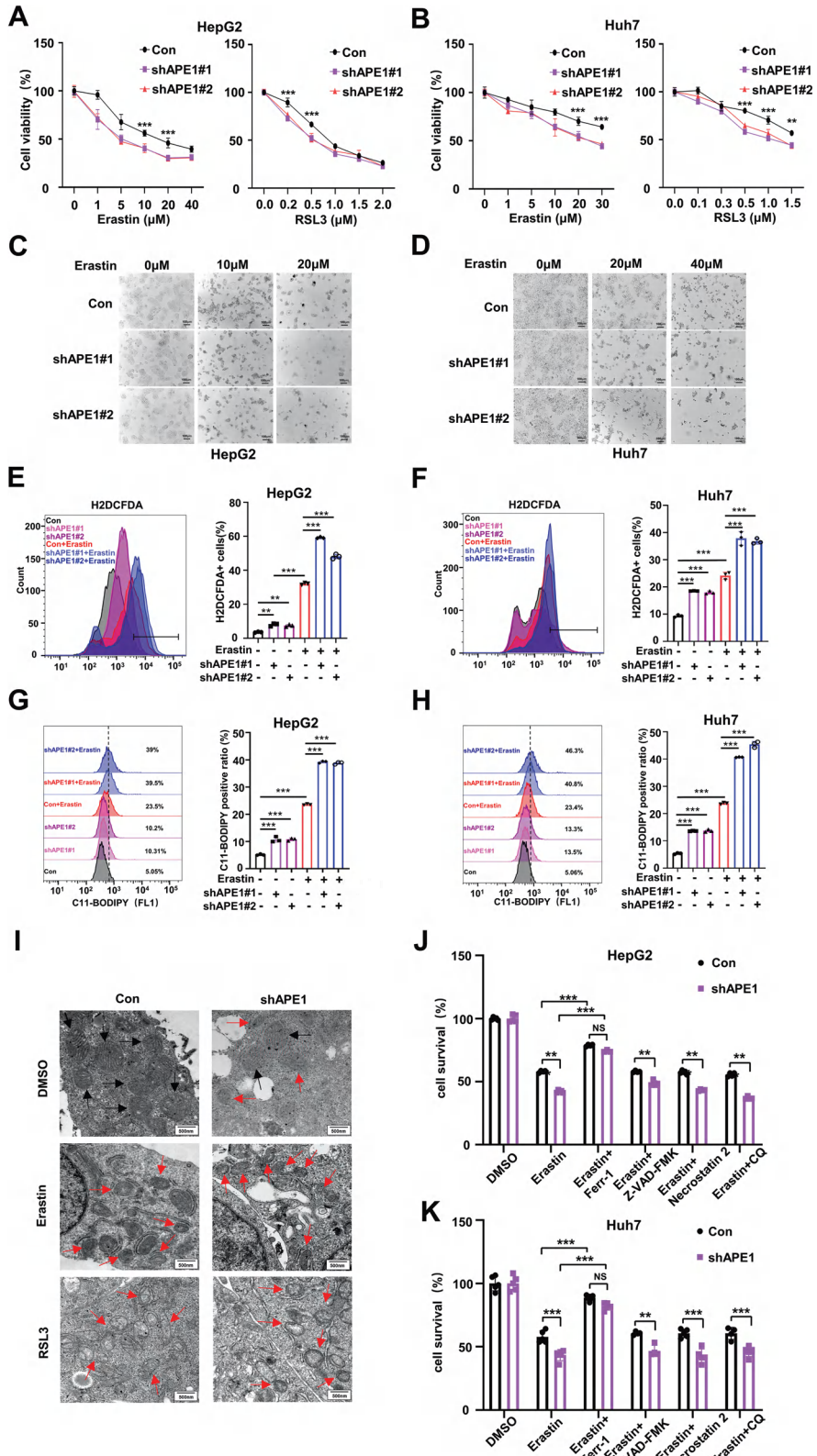
Recently, many studies have shown that ferroptosis is related to the development and therapeutic response of HCC [10]. Previous studies have also found high expression of APE1 in HCC, which contributed to HCC progression and associated with its poor prognosis [30]. Due to the multifunction of APE1 and its role in HCC, we wonder whether APE1 was involved in ferroptosis in HCC. Two APE1-knockdown (APE1-KD) HCC cell lines were generated based on HepG2 and Huh7 cells (Supplementary Fig. S1A, B). We found the knockdown of APE1 promoted the susceptibility of HCC cells to ferroptosis induced by erastin and RSL3 (Fig. 1A–D; Supplementary Fig. S1C, D). We next investigated intracellular levels of ROS and lipid peroxidation, which are two markers associated with ferroptosis. H2DCFDA and C11-BODIPY 581/591 staining were employed to assess these levels in both control and APE1-KD cells, and we observed a significant increase in intracellular ROS and lipid peroxidation levels upon treatment with erastin and RSL3 in APE1-KD cells (Fig. 1E–H; Supplementary Fig. S1E–H). Further analysis using transmission electron microscopy revealed that mitochondria in APE1-KD cells under the treatments of erastin or RSL3 exhibited morphological changes associated with significant ferroptosis, including smaller mitochondria, increased membrane density, reduced cristae, and mitochondrial fragmentation (Fig. 1I). Our results suggest that APE1 inhibition promotes erastin- and RSL3-induced ferroptosis in HCC cells.

Previous studies, including our own, have demonstrated that inhibition of APE1 induces a variety of cell deaths, such as apoptosis, pyroptosis, and necroptosis [21, 26]. To further confirm the mode of cell death promoted by the knockdown of APE1 in HCC cells under erastin or RSL3 treatments, we treated cells with different cell death inhibitors, such as ferroptosis inhibitor ferrostatin-1 (Ferr-1), apoptosis inhibitor Z-VAD-FMK, necroptosis inhibitor Necrostatin 2, and autophagy inhibitor CQ. Only Ferr-1 reversed APE1-KD-induced cell death, while Z-VAD-FMK, Necrostatin 2, and CQ showed no effect in these detections (Fig. 1J, K; Supplementary Fig. S1I, J). Morphological observations also revealed that Ferr-1 was able to reverse the ferroptosis promoted by APE1 knockdown (Supplementary Fig. S2A–D). In addition, we observed that Ferr-1 reversed the APE1-KD-induced intracellular ROS and lipid peroxidation levels in HCC with erastin and RSL3 treatments (Supplementary Fig. S2E–L). These findings suggest that APE1 inhibition promotes erastin- and RSL3-induced ferroptosis.

To confirm the effect of APE1 on ferroptosis in HCC cells, we further constructed plasmids overexpressing APE1 (APE1-OV) (Supplementary Fig. S3A). Our results showed that APE1 overexpression in HCC cells all inhibited erastin- and RSL3-induced ferroptosis as well as increased intracellular ROS and lipid peroxidation levels (Supplementary Fig. S3B–K). Taken together, these findings indicate that APE1 plays a crucial role as a regulator of ferroptosis in HCC and that inhibition of APE1 promotes ferroptosis in HCC cells.

APE1 regulates ferroptosis through NRF2/SLC7A11/GPX4 axis

To investigate the underlying molecular mechanisms by which APE1 inhibition promotes ferroptosis, we examined the expression of key genes involved in the ferroptosis pathway, including



SLC7A11, GPX4, FSP1, ACSL4, and FTL [31]. Our results revealed that only mRNA levels of SLC7A11 and GPX4 were significantly downregulated in APE1-KD HCC cells (Fig. 2A, B; Supplementary Fig. S4A, B). Western blotting analysis confirmed the protein levels of SLC7A11 and GPX4 decreased in APE1-KD cells compared to

control cells (Fig. 2C, D). Previous studies have demonstrated that the expression of SLC7A11 and GPX4 is regulated by transcription factors, NRF2, p53, and HIF-1 α during ferroptosis [3, 12, 32, 33]. In order to determine how APE1 regulates the expression of SLC7A11 and GPX4, we examined the role of APE1 in modulating

Fig. 1 Inhibition of APE1 promotes ferroptosis in HCC cells. **A, B** CCK-8 assay of cell viability in control and APE1-KD HepG2 and Huh7 cells after treatment with different concentrations of erastin and RSL3 for 24 h. **C, D** Morphological analysis of control and APE1-KD HepG2 and Huh7 cells after treatment with different doses of erastin for 24 h. **E, F** ROS levels in control and APE1-KD cells were detected using H2DCFDA staining in HCC cells after treatment with or without erastin (10 μ M for HepG2 and 20 μ M for Huh7) for 24 h. **G, H** Lipid peroxidation levels in control and APE1-KD cells were detected using C11-BODIPY staining in HCC cells after treatment with or without erastin (10 μ M for HepG2 and 20 μ M for Huh7) for 24 h. **I** The morphology of intracellular mitochondria was observed by TEM after treatment of control and APE1-KD HepG2 cells with or without 10 μ M erastin or 0.5 μ M RSL3 for 24 h. The black arrows indicated the normal mitochondria. The red arrows indicated the abnormal mitochondria. **J, K** CCK-8 assay of cell viability in control and APE1-KD HCC cells after treatment with erastin (10 μ M for HepG2 and 20 μ M for Huh7) \pm indicated inhibitors (1 μ M Ferrostatin-1, 5 μ M Z-VAD-FMK, 2 μ M Necrostatin-2, or 2 μ M CQ) for 24 h. Data are shown as the mean \pm SD ($n = 3$). ** $P < 0.01$, *** $P < 0.001$.

these transcription factors. We found that the knockdown of APE1 downregulated the protein levels of NRF2, but not HIF-1 α and p53 in HCC cells (Fig. 2C, D). Moreover, overexpression of NRF2 (NRF2-OV) restored the downregulation of SLC7A11 and GPX4 caused by APE1 inhibition in HCC cells (Fig. 2E, F; Supplementary Fig. S4C–F). Our results also showed that the combined knockdown of APE1 and NRF2 resulted in a similar reduction in the expression of SLC7A11 and GPX4 compared to the individual knockdown of APE1 or NRF2 (Fig. 2G, H; Supplementary Fig. S4G–J). In addition, overexpression of NRF2 could upregulate the mRNA levels of SLC7A11 and GPX4, while knockdown of NRF2 could downregulate the mRNA levels of SLC7A11 and GPX4 in HCC cells (Supplementary Fig. S4K–N), consistent with previous studies [12, 34]. These findings suggest that APE1 regulates the expression of SLC7A11 and GPX4 by modulating the transcription factor NRF2.

APE1 inhibition promotes NRF2 degradation via the AKT/GSK3 β -mediated ubiquitin/proteasome pathway

As mentioned above, the knockdown of APE1 downregulated NRF2 protein levels in HCC cells prompting us to investigate the mechanism underlying the regulation of NRF2 by APE1. First, we examined the changes of NRF2 mRNA levels after the knockdown of APE1. Interestingly, the knockdown of APE1 did not affect the mRNA levels of NRF2 in HCC cells (Supplementary Fig. S5A, B). Then, we examined the protein stability of NRF2. We used the protein synthesis inhibitor cycloheximide (CHX) to detect the effect of APE1 on NRF2 protein stability and found that NRF2 protein degraded more rapidly in APE1-KD cells compared to those in control cells (Fig. 3A, B). Moreover, the proteasome inhibitor MG132 reversed the regulatory effect of APE1 on NRF2 protein levels (Fig. 3C, D). Previous studies have found that the stability of NRF2 protein is mainly regulated by KEAP1; KEAP1 forms a ubiquitin E3 ligase complex with CULLIN3 (CUL3) to ubiquitinate NRF2, leading to its degradation by the proteasome [35]. However, the knockdown of APE1 did not affect the protein levels of KEAP1 in HCC cells (Fig. 3E, F). In addition, the stability of NRF2 protein can be regulated in a KEAP1-independent manner; it has been found that NRF2 can be phosphorylated by glycogen synthase kinase-3 β (GSK3 β), which in turn is recognized by beta-transducin repeat-containing protein (β -TrCP) and ubiquitinated by the β -TrCP/Cul1 E3 ligase complex, and finally degraded by the proteasome [36]. Although the knockdown of APE1 did not affect the GSK3 β (active) protein level, the phosphorylated GSK3 β (inactive) protein level was significantly downregulated in response to APE1 inhibition (Fig. 3E, F). Furthermore, the use of AR-A014418, an inhibitor of GSK3 β , restored the downregulation of NRF2 caused by APE1 inhibition in HCC cells (Supplementary Fig. S5C, D). To further explore whether APE1 inhibition promotes NRF2 ubiquitination via GSK3 β , GSK3 β inhibitor AR-A01448 or siGSK3 β were applied. Our data showed that the ubiquitination level of NRF2 was upregulated in APE1-KD cells, while AR-A014418 treatment or knockdown of GSK3 β by siGSK3 β were able to reverse this increase in NRF2 ubiquitination (Fig. 3G, H; Supplementary Fig. S5E–J). And by CHX assay we found that the degradation rate of NRF2 was the same in control and APE1

knockdown groups after using AR-A01148 or knockdown of GSK3 β (Fig. 3I, J; Supplementary Fig. S5K, L). Moreover, we found that E3330, an inhibitor specifically targeting the redox function of APE1, reduced NRF2 protein levels, which could be restored by treatment with MG132 (Supplementary Fig. S5M, N). Interestingly, CRT0044876 (CRT), a DNA damage repair function-specific APE1 inhibitor, was not able to down-regulate NRF2 protein levels (Supplementary Fig. S5O, P).

Next, we further explored the specific mechanism by which APE1 regulates GSK3 β . Previous studies have shown that GSK3 β is a downstream substrate and effector of AKT [37]. We found that the knockdown of APE1 or treatment of cells with E3330 did not impact the protein level of AKT, but significantly downregulated the protein level of p-AKT (Ser473) (Fig. 3K, L). The unphosphorylated form of AKT was virtually inactive and phosphorylation of Ser-473 stimulated its activity [38]. Previous studies have demonstrated that the redox state of AKT plays a crucial role in its activation. Inactive AKT can form redox-sensitive intramolecular disulfide bonds between Cys-297 and Cys-311 in the kinase structural domain, which consequently impairs AKT phosphorylation [38]. In addition, APE1 is a redox protein that can affect the activity of proteins such as AP-1, NF- κ B, STAT3, and HIF1 α by modulating the redox state of cysteine residues [13]. Interestingly, we found that knockdowns of APE1 or treatment of cells with E3330 resulted in a significant increase in oxidative state AKT (Fig. 3M, N). These data implied that APE1 is involved in ferroptosis by affecting GSK3 β activity through AKT and thus regulating NRF2 stability. To confirm this hypothesis, Ipatasertib, an ATP-competitive AKT inhibitor, or knockdown of AKT were applied for further experiments. We found that Ipatasertib or knockdown of AKT significantly inhibited the phosphorylation of GSK3 β and reduced the protein level of NRF2. Moreover, inhibition of AKT significantly inhibited the upregulated phosphorylation of levels GSK3 β and the NRF2 protein level caused by APE1 overexpression (Fig. 3O, P; Supplementary Fig. S5Q, V). These data suggest that APE1 was able to regulate the reduced state of AKT protein in cells, thereby modulating the phosphorylation and activation of AKT. In conclusion, the above results suggest that inhibition of APE1 impairs the stability of NRF2 protein by increasing oxidative AKT, leading to downstream GSK3 β to be activated via dephosphorylation, which in turn triggers NRF2 degradation via the ubiquitin/proteasome pathway.

APE1 inhibition-enhanced ferroptosis is NRF2-dependent

To further confirm the role of NRF2 in APE1 inhibition-enhanced ferroptosis, we overexpressed NRF2 in control or APE1-KD HCC cells. Notably, overexpressing NRF2 overcome the APE1 inhibition-enhanced ferroptosis in HCC cells, which was induced by erastin or RSL3 (Fig. 4A, B; Supplementary Fig. S6A, B). These results were confirmed by morphological analysis (Fig. 4C, D; Supplementary Fig. S6C, D). In addition, NRF2 overexpression downregulated erastin- and RSL3-stimulated intracellular ROS and lipid peroxidation levels in HCC cells and reversed the potentiating effect of APE1 deletion (Fig. 4E–H; Supplementary Fig. S6E–H). Moreover, we further experimented with the knockdown of NRF2 on basis of the APE1 knockdown. We found that the knockdown of APE1 alone or NRF2 alone promoted a similar rate of ferroptosis as the

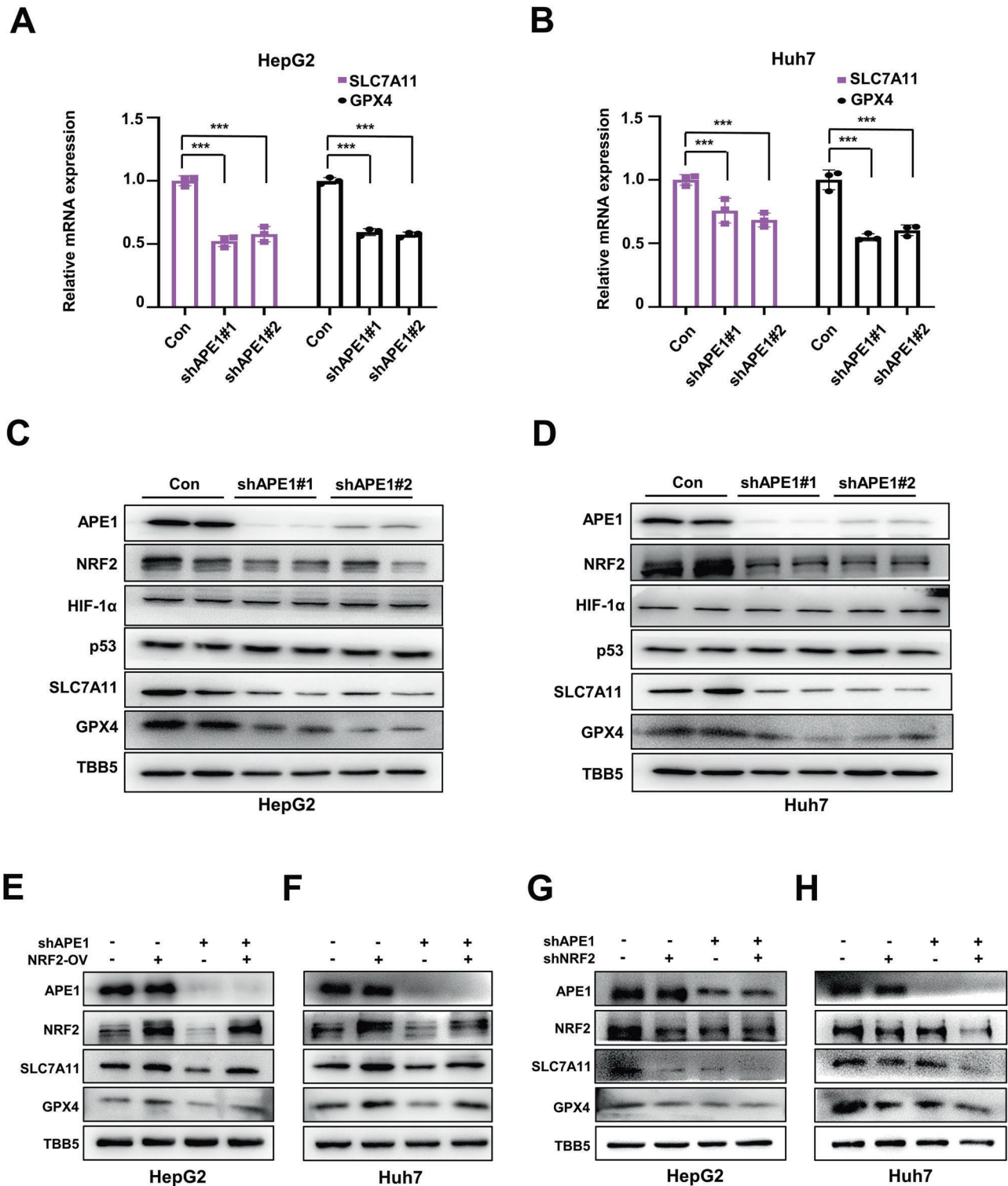
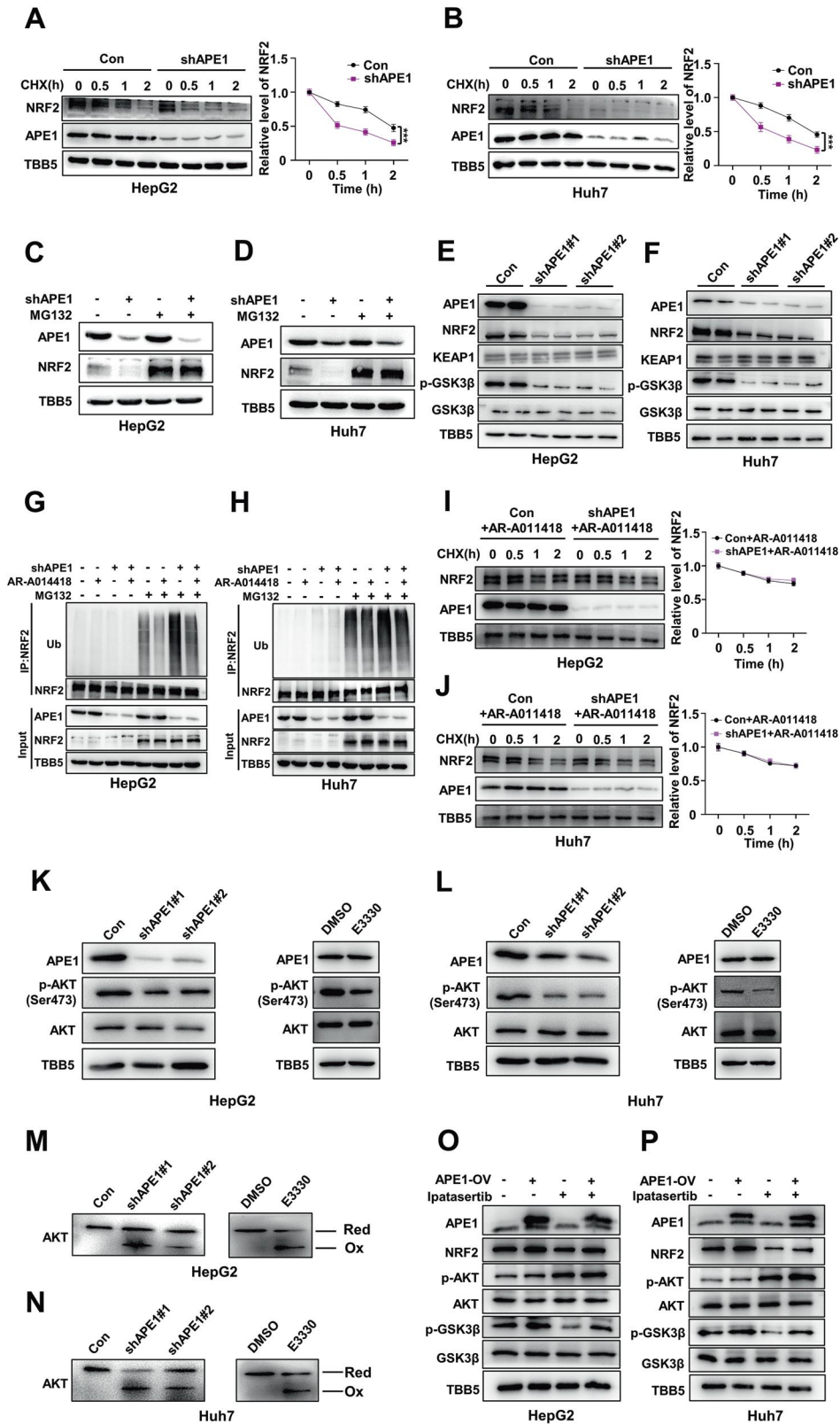


Fig. 2 APE1 regulates ferroptosis through NRF2/SLC7A11/GPX4 axis. **A, B** The mRNA levels of SLC7A11 and GPX4 in control and APE1-KD HepG2 and Huh7 cells were detected by qRT-PCR. **C, D** Protein levels of APE1, NRF2, HIF-1 α , p53, SLC7A11, and GPX4 were analyzed by western blotting in control and APE1-KD HepG2 and Huh7 cells. **E, F** Protein levels of SLC7A11 and GPX4 after NRF2-OV in control and APE1-KD HepG2 and Huh7 cells were. **G, H** Protein levels of SLC7A11 and GPX4 after NRF2 knockdown in control and APE1-KD HepG2 and Huh7 cells. Data are shown as the mean \pm SD ($n = 3$). *** $P < 0.001$.

co-knockdown of both APE1 and NRF2 in HCC cells with erastin or RSL3 treatment (Fig. 4I, J; Supplementary Fig. S6I, J). In conclusion, our data suggest that the regulation of APE1 on ferroptosis is NRF2 dependent.

Ferroptosis promoted by APE1 inhibition is independent of its DNA repair function

Given that APE1 has both DNA repair functions and redox signaling regulation functions mediated by its two domains, we



wondered which specific function of APE1 is involved in the regulation of ferroptosis. First, we confirmed the upregulation of DNA damage levels in APE1-KD HCC cells. As expected, the knockdown of APE1 or the use of CRT increased the γ -H2AX levels, a DNA damage marker, in HCC cells (Fig. 5A–D). However, Ferr-1,

which was able to rescue APE1 inhibition-enhanced ferroptosis, did not affect the γ -H2AX levels in APE1-KD cells or cells with CRT treatment, as well as those in control cells (Fig. 5A–D). In addition, Ferr-1 treatment did not affect the protein levels of DNA damage response signals such as p-CHK2 (Fig. 5A–D). Immunofluorescence

Fig. 3 APE1 regulates the stability of NRF2 through GSK3 β -involved ubiquitination/proteasome pathway. **A, B** Protein levels of NRF2 were analyzed by western blotting in control and APE1-KD HepG2 and Huh7 cells after treatment with CHX (100 μ g/ml) at different times (left). The quantification of NRF2 degradation rate by grayscale analysis (right). **C, D** Protein levels of NRF2 in control and APE1-KD HepG2 and Huh7 cells were analyzed by western blotting with or without MG132 (10 μ M) treatment for 6 h. **E, F** Protein levels of APE1, NRF2, KEAP1, p-GSK3 β , and GSK3 β were analyzed by western blotting in control and APE1-KD HepG2 and Huh7 cells. **G, H** Ubiquitinated NRF2 in control and APE1-KD HepG2 and Huh7 cells after treatment with or without AR-A014418 (20 μ M) and with or without MG132 (10 μ M) for 6 h were analyzed by immunoprecipitation with anti-NRF2 antibody and immunoblotting with anti-ubiquitin antibody. **I, J** Protein levels of NRF2 were analyzed by Western blotting after treatment of control and APE1-KD HepG2 and Huh7 cells with AR-A01448 (20 μ M) for 6 h, followed by treatment with CHX (100 μ g/ml) for different times (left). The quantification of NRF2 degradation rate were calculated by grayscale analysis (right). **K, L** Protein levels of APE1, p-AKT (Ser473), and AKT were analyzed by western blotting in control and APE1-KD HepG2 and Huh7 cells or in HepG2 and Huh7 cells after treatment with E3330 (50 μ M) for 24 h. **M, N** The redox state of the protein of AKT was analyzed by Western blotting in control and APE1-KD HepG2 and Huh7 cells or in HepG2 and Huh7 cells after treatment with E3330 (50 μ M) for 24 hours. The positions of reduced (Red) and oxidized (Ox) proteins are indicated. **O, P** Protein levels of APE1, NRF2, p-AKT (Ser473), AKT, p-GSK3 β , and GSK3 β were analyzed by western blotting of protein levels in cells from control and APE1-OV HepG2 and Huh7 cells after treatment with or without Ipatasertib (2 μ M) for 24 h. Data are shown as the mean \pm SD ($n = 3$). *** $P < 0.001$.

assay consistently showed that the knockdown of APE1 or use of CRT increased the γ -H2AX foci numbers, which were not changed after Ferr-1 treatment (Fig. 5E–H). Moreover, we combined CRT with erastin and RSL3 to treat HCC cells and found that CRT showed no effect on ferroptosis in HCC cells induced by erastin and RSL3 (Fig. 5I–L). This is also consistent with our previous experimental results that treatment of HCC cells with CRT does not affect intracellular NRF2 protein levels. These results suggested that APE1 inhibition-enhanced ferroptosis is independent of its DNA repair function.

We further investigate whether the ferroptosis inducers erastin and RSL3 show on DNA damage. WB assay, showed that erastin and RSL3 could not induce the accumulation of γ -H2AX protein levels in HCC cells, whereas the Adriamycin (a tumor chemotherapeutic agent that induces DNA damage) significantly induced γ -H2AX upregulation (Supplementary Fig. S7A, B). Consistently, immunofluorescence showed that erastin and RSL3 did not induce the formation of γ -H2AX and 53BP1 foci compared to negative control (Supplementary Fig. S7C, F). These results suggest that ferroptosis inducers do not induce DNA damage in HCC cells.

APE1 regulates ferroptosis dependent on its redox function

To determine whether the redox function of APE1 is involved in the regulation of ferroptosis, we treated HCC cells with the E3330 and found that E3330 treatment enhanced cell death induced by erastin and RSL3 (Fig. 6A, B; Supplementary Fig. S8A, B). Furthermore, E3330 treatment downregulated the mRNA and protein levels of SLC7A11 and GPX4, as well as the protein levels of NRF2 in HCC cells (Fig. 6C, D; Supplementary Fig. S8C, D). We further constructed a DNA damage repair function mutant (H309N) and a redox function mutant (C65A) of APE1 (Supplementary Fig. S8E, F). We found that overexpression of WT APE1 and APE1-H309N, but not APE1-C65A, increased the protein levels of NRF2, SLC7A11, and GPX4 compared to the control group (Fig. 6E, F). In addition, overexpression of APE1 and APE1-H309N increased the mRNA levels of SLC7A11 and GPX4 (Supplementary Fig. S8G, H). Furthermore, overexpression of WT APE1 and APE1-H309N, but not APE1-C65A, in APE1-KD cells rescued the mRNA and protein levels of SLC7A11 and GPX4, as well as NRF2 protein level (Fig. 6G, H; Supplementary Fig. S8I, J).

We next focused on whether the redox function of APE1 is involved in regulating the phosphorylation of GSK3 β , which in turn affects the protein stability of NRF2. We found that the protein levels of p-GSK3 β and NRF2 were significantly reduced when cells were treated with E3330 (Fig. 6I, J). In addition, overexpression of APE1 significantly increased the protein levels of p-GSK3 β and NRF2, while APE1-C65A did not (Fig. 6K, L). These data suggest that APE1 regulates the phosphorylation of GSK3 β through its redox function, which affects the stability of NRF2 and regulates the expression of SLC7A11 and GPX4 involved in ferroptosis.

APE1 inhibition enhances the sensitivity of HCC to ferroptosis in vivo

To further investigate the effects of APE1 inhibition on ferroptosis of HCC in vivo, we established an APE1-KD Huh7-derived xenograft model in nude mice (Fig. 7A). While both APE1-KD and erastin treatment individually impeded tumor growth compared to the control groups, the combination of APE1-KD and erastin treatment resulted in an enhanced therapeutic effect (Fig. 7B–D; Supplementary Fig. S9A). We examined lipid peroxidation levels by flow cytometry and found that inhibition of APE1 upregulated the levels of lipid peroxidation induced by erastin in tumor tissues (Fig. 7E). IHC staining and WB experiments showed that erastin treatment increased the protein levels of SLC7A11 and CHAC1, suggesting that erastin is effective for treatment in mice (Fig. 7F; Supplementary Fig. S9B, C). In addition, NRF2, SLC7A11 and GPX4 protein levels were decreased in APE1-KD Huh7 cell-derived tumor tissues compared to those from WT Huh7-derived tumor tissues, which was consistent with the in vitro data (Fig. 7F; Supplementary Fig. S9B). And knockdown of APE1 significantly upregulated the accumulation of erastin-induced 4-HNE, a lipid peroxidation marker, in tumor tissues (Fig. 7F). Taken together, these results suggest that APE1 deletion enhances the therapeutic effect of erastin on HCC in vivo.

Expression pattern of APE1, SLC7A11, GPX4, and NRF2 is clinically associated with the progression and prognosis of HCC

To further evaluate the functional interaction among APE1 and ferroptosis genes, SLC7A11, GPX4, and NRF2, we carried out translational studies using tissue microarray collected from HCC patients' samples (Supplementary Table S3). The IHC data showed that the expression levels of APE1, NRF2, SLC7A11, and GPX4 were all higher in HCC tissues compared to those in paraneoplastic tissues (Fig. 8A–D). Notably, the expression levels of APE1 were positively correlated with the expression levels of NRF2, SLC7A11, and GPX4 (Fig. 8E–G). In addition, the expression of APE1 was further analyzed using the public data from TCGA and GTEx databases. The mRNA level of APE1 was significantly increased in HCC tissue samples compared to normal tissues (Fig. 8H). Furthermore, the gene expression profiles of 48 liver cancer tissues and 39 non-cancerous tissues from 61 patients were analyzed using the GEO database, and a high expression of APE1 in liver cancer tissues was detected (Supplementary Fig. S10A). In addition, HCC patients with higher APE1 expression levels showed poorer overall survival than those with lower APE1 expression levels (Fig. 8I). The expression levels of SLC7A11 and GPX4 were found to be higher in HCC samples compared to normal tissues, as indicated by the data obtained from TCGA and GTEx databases (Fig. 8J, K). Further analysis of Spearson's correlation coefficients revealed a positive correlation between the expression levels of APE1 and SLC7A11 as well as GPX4 in both HCC and normal tissues, based on the data obtained from TCGA and GTEx databases (Supplementary Fig. S10B, C). Finally, GEO data showed that the mRNA level of APE1 was significantly

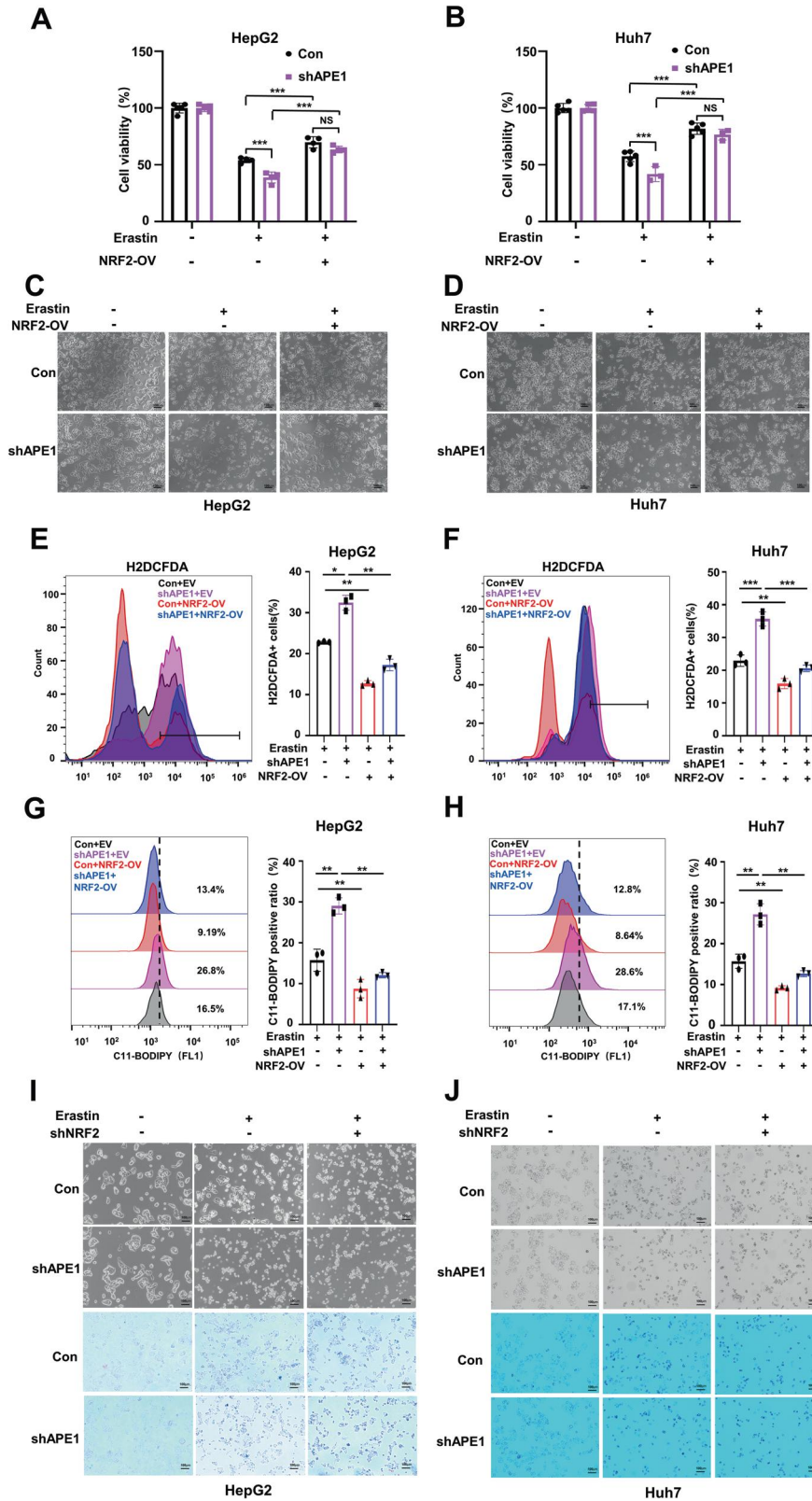
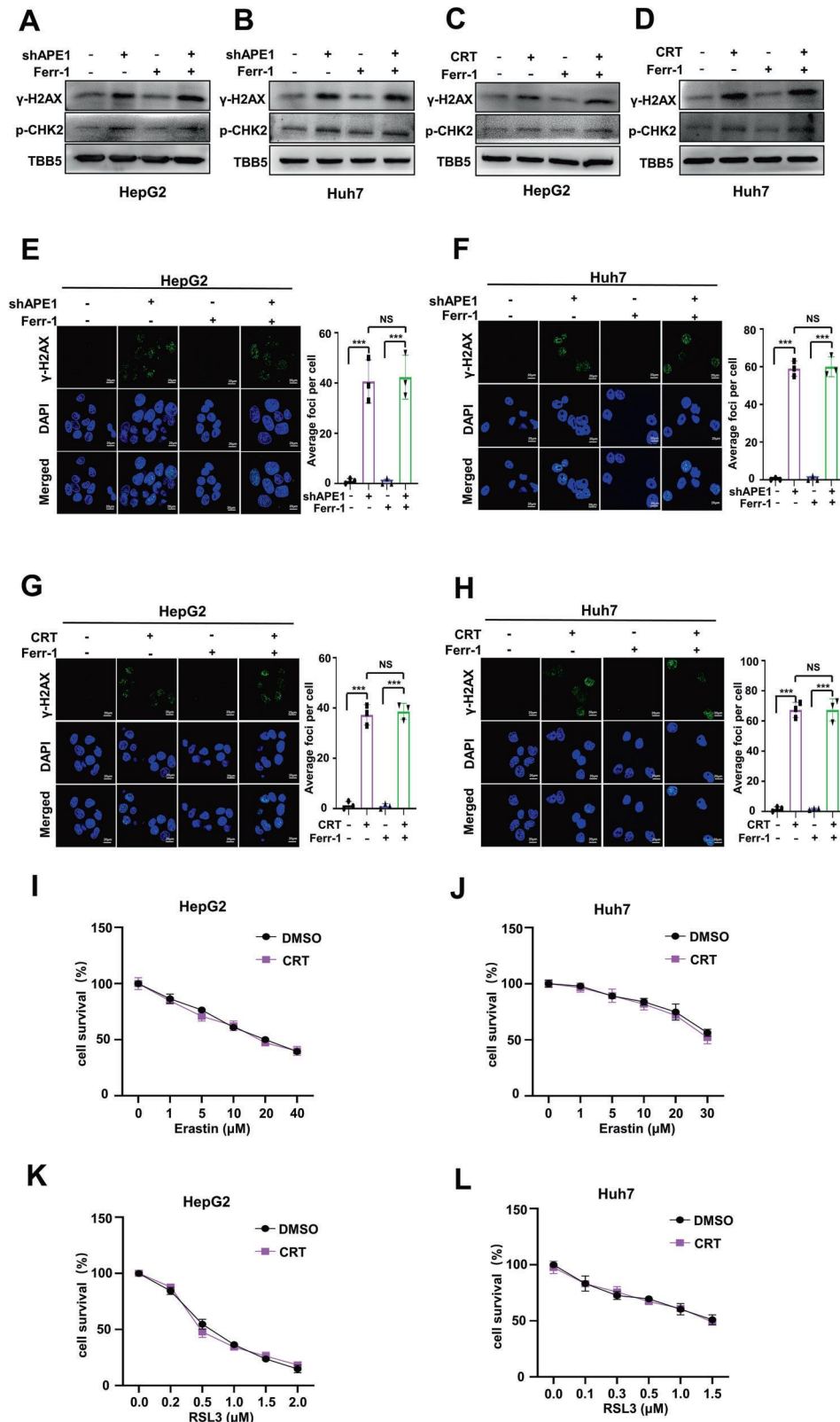


Fig. 4 APE1-modulated ferroptosis is NRF2-dependent. **A, B** CCK-8 assay of cell viability after overexpression of NRF2 in control and APE1-KD HCC cells after treatment with erastin (10 μM for HepG2 and 20 μM for Huh7) for 24 h. **C, D** Morphological analysis of cells after overexpression of NRF2 in control and APE1-KD HCC cells after treatment with erastin (10 μM of HepG2 and 20 μM of Huh7) for 24 h. **E, F** After overexpression of NRF2 in control and APE1-KD HCC cells, the cells were after treatment with erastin (10 μM of HepG2 and 20 μM of Huh7) for 24 h and stained with H2DCFDA to detect the ROS level of the cells. **G, H** After overexpression of NRF2 in control and APE1-KD HCC cells, the cells were after treatment with erastin (10 μM of HepG2 and 20 μM of Huh7) for 24 h and stained with C11-BODIPY to detect the Lipid peroxidation level of the cells. **I, J** Morphological analysis and trypan blue assay of cells after knockdown of NRF2 in control and APE1-KD HCC cells after treatment with erastin (10 μM of HepG2 and 20 μM of Huh7) for 24 h. Data are shown as the mean ± SD (*n* = 3). **P* < 0.05, ***P* < 0.01, ****P* < 0.001.



downregulated in HepG2 cells in response to the ferroptosis inducer erastin (Supplementary Fig. S10D). In summary, the above data suggest that APE1 was involved in the progression of human HCC and participated in HCC ferroptosis, which further elevated the clinical value of APE1 in HCC therapy through its regulatory role in ferroptosis.

DISCUSSION

Ferroptosis is a recently discovered form of cell death, and emerging studies show that ferroptosis plays an important role in anti-tumor processes [39–41]. In the present study, we revealed that APE1 deficiency promoted cell death induced by the

Fig. 5 The DNA damage repair function of APE1 is not involved in ferroptosis. **A, B** Protein levels of γ -H2AX were analyzed by Western blotting in control and APE1-KD HepG2 and Huh7 cells after treatment with or without 1 μ M of Ferrostatin-1 for 24 h. **C, D** Protein levels of γ -H2AX were analyzed by Western blotting in HepG2 and Huh7 cells after treatment with Ferrostatin-1 (1 μ M) or CRT (100 μ M) or CRT in combination with Ferrostatin-1 for 24 h. **E, F** Immunofluorescence analysis of γ -H2AX foci in control and APE1-KD HepG2 and Huh7 cells after treatment with or without 1 μ M of Ferrostatin-1 for 24 h. The quantification of average foci numbers per cell are shown in the right panel, 50 cells were calculated in each group. **G, H** Immunofluorescence analysis of γ -H2AX foci in HepG2 and Huh7 cells after treatment with Ferrostatin-1 (1 μ M) or CRT (100 μ M) or CRT in combination with Ferrostatin-1 for 24 h. The quantification of average foci numbers per cell are shown in the right panel, 50 cells were calculated in each group. **I, J** CCK-8 assay of cell viability in HepG2 and Huh7 cells after treatment with different concentrations of erastin \pm 100 μ M CRT for 24 h. **K, L** CCK-8 assay of cell viability in HepG2 and Huh7 cells after treatment with different concentrations of RSL3 \pm 100 μ M CRT for 24 h. Data are shown as the mean \pm SD ($n = 3$). *** $P < 0.001$.

ferroptosis inducer erastin and RSL3. Further studies demonstrated that the knockdown of APE1 promoted ferroptosis by regulating the NRF2/SLC7A11/GPX4 axis. APE1 inhibition increases AKT in the oxidized state, inhibiting its phosphorylation and activation, allowing downstream GSK3 β to be activated via dephosphorylation, further promoting the degradation of NRF2 in the ubiquitin/proteasome pathway, leading to downregulation of SLC7A11 and GPX4. Our study establishes APE1 as a regulator of ferroptosis, and suggests that targeting APE1 to promote ferroptosis may be a promising therapeutic strategy for the treatment of HCC (Fig. 8L).

Ferroptosis is caused by lipid peroxidation due to ROS accumulation [2]. The unique metabolism of tumor cells, which is more dependent on antioxidant mechanisms, causes them to be more susceptible to oxidative stress and ferroptosis [42–44]. Numerous studies have demonstrated that ferroptosis can be triggered by treatments for cancer such as radiotherapy, chemotherapy, and immunotherapy [4, 12, 41]. Many studies have shown that APE1 is widely involved in various diseases caused by oxidative stress, and overexpression of APE1 enhances cellular resistance to oxidative stress while reducing intracellular ROS levels [15, 45]. Moreover, this study suggests that the inhibition of APE1 can increase intracellular ROS levels and promote the accumulation of lipid peroxidation products triggered by the ferroptosis inducer erastin and RSL3, thereby further promoting ferroptosis. Knockdown of APE1 exhibited morphological characteristics consistent with ferroptosis, including pronounced mitochondrial condensation and disappearance of mitochondrial cristae, as observed by transmission electron microscopy. Further studies revealed that overexpression of APE1 inhibited erastin- and RSL3-induced ferroptosis as well as the rise in intracellular ROS and lipid peroxidation levels. In addition, we found that APE1 inhibition-enhanced cell death could be reversed by ferrostatin-1, but not by Z-VAD-FMK, Necrostatin 2, or CQ. This indicates that the APE1 inhibition-enhanced cell death observed in HCC cells is attributed to ferroptosis. Consistently, a recent study found that sustained oxidative stress during ferroptosis upregulates APE1 expression thereby increasing the resistance of tumor cells to ferroptosis [28]. Combining our data, the usage of APE1 redox activity was a potential strategy to solve ferroptosis resistance in HCC and other cancers. In according with our previous study, which showed that molecule inhibition of APE1 induced several other kinds of cell death such as apoptosis, pyroptosis, and necroptosis, we demonstrated that APE1 is a regulator of multiple cell death factors.

Ferroptosis can be regulated by various factors, such as SLC7A11, GPX4, FSP1, ACSL4, and FTL [7, 8, 46–48]. Our study found that APE1 affected the expression of SLC7A11 and GPX4, which are key regulators of ferroptosis inhibition. Recently, it has been shown that APE1 is able to regulate iron death through p53 in GC cells [27]. However, we further found that knockdown of APE1 in HCC cells did not alter the level of p53, but significantly downregulated the protein level of NRF2. NRF2 is a stress-inducible transcription factor with an antioxidant function that is directly associated with ferroptosis sensitivity [49]. Our study showed that the inhibition of APE1 reduced the protein level of NRF2, and further downregulated

the expression of SLC7A11 and GPX4, whereas overexpression of NRF2 restored its expression and inhibited ferroptosis. Interestingly, APE1 did not affect the level of NRF2 transcripts, but rather the protein level. The stability of NRF2 protein is normally regulated by its physiological inhibitor KEAP1, which keeps it undergoing rapid ubiquitination and further degradation via the proteasome [35]. However, we found that the knockdown of APE1 did not affect KEAP1 levels. Alternatively, NRF2 can be degraded independently by KEAP1, such as the now-recognized NRF2 negative regulator GSK3 β . It was found that GSK3 β is able to phosphorylate NRF2, which is subsequently recognized by β -TrCP, leading to ubiquitination and proteasomal degradation [36, 50]. Our study found that inhibition of APE1 significantly reduced the p-GSK3 β (inactive) levels thus increasing GSK3 β activity, resulting in a downregulation of NRF2 protein levels in the ubiquitin/proteasome pathway, which is consistent with previous study [30]. While NRF2 degradation via the proteasome pathway occurs in the cytoplasm and APE1 was primary recognized as nucleolus protein, a number of studies have shown that APE1 is also localized in the cytoplasm and mitochondria, especially that the distribution of APE1 in the cytoplasm is much higher in HCC tissues than in normal liver tissues [51, 52]. This suggests that APE1 is able to regulate NRF2 stability in the cytoplasm, thereby regulating the expression of SLC7A11 as well as GPX4. In addition, GSK3 β serves as a significant downstream target of AKT, and our study revealed that inhibiting APE1 resulted in reduced phosphorylation and activation of AKT. Prior research has established the importance of the redox state in AKT phosphorylation and activation. Specifically, the formation of intramolecular disulfide bonds between Cys-297 and Cys-311 in the structural domain of oxidized AKT kinase inhibits its phosphorylation and subsequent activation [37]. Interestingly, we found that inhibition of APE1 increased AKT in the oxidized state. This suggests that APE1, as a redox protein, regulates the redox state of AKT and thus its phosphorylation and activation. Previous study reported that APE1 could regulate AKT signaling to overcome the resistance of lung adenocarcinoma (LUAD) cells to epithelial growth factor receptor-tyrosine kinase inhibitors (EGFR-TKIs) [53]. Our study also demonstrated the key role of APE1 on regulation of AKT signaling. Overall, our experiments demonstrate that APE1 regulates the expression of the SLC7A11 and GPX4 through AKT/GSK3 β /NRF2 pathway involved in ferroptosis in HCC cells.

APE1 is a multifunctional protein that possesses both DNA damage repair and redox functions, and the two functions are independent of each other [15]. Thus, APE1 is involved in the regulation of multiple cellular processes, including DNA damage response, oxidative stress, cell cycle, and cell death [15, 54]. It serves as a core protein in base excision repair, and its deletion or inhibition of DNA damage repair function leads to the accumulation of DNA damage in cells, which results in cellular senescence or death [26, 55]. Although the hypothesis of DNA damage in driving ferroptosis remains intriguing, the DNA damage responses in ferroptosis are context-dependent [56]. Our study showed that the DNA damage repair function of APE1 is not involved in the regulation of ferroptosis. This finding is consistent with previous studies that the ionizing radiation (IR)-induced DNA damage response did not correlate with ferroptosis [41]. Although some

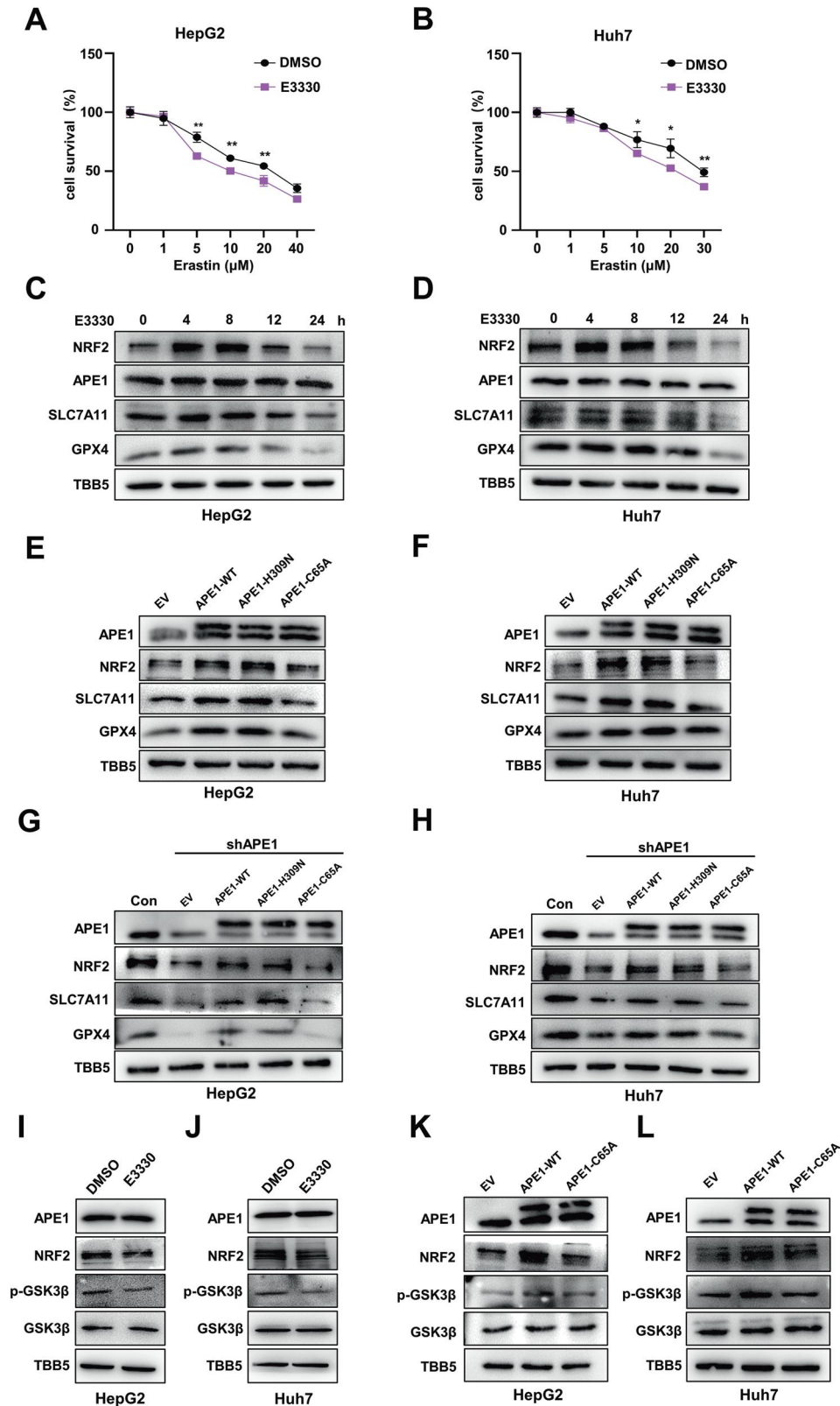


Fig. 6 APE1 relies on its redox function to participate in ferroptosis. **A, B** CCK-8 assay of cell viability in HepG2 and Huh7 cells after treatment with different concentrations of erastin \pm 50 μ M E3330 for 24 h. **C, D** Protein levels of APE1, NRF2, SLC7A11, and GPX4 were analyzed by western blotting in HepG2 and Huh7 cells after treatment with E3330 (50 μ M) for 0, 4, 8, 12, and 24 h. **E, F** Protein levels of APE1, NRF2, SLC7A11, and GPX4 in HepG2 and Huh7 cells after overexpression of APE1-WT, APE1-H309N, and APE1-C65A were analyzed by western blotting. **G, H** Protein levels of APE1, NRF2, SLC7A11, and GPX4 in APE1-KD HepG2 and Huh7 cells after overexpression of APE1-WT, APE1-H309N, and APE1-C65A were analyzed by western blotting. **I, J** Protein levels of APE1, NRF2, p-GSK3 β , and GSK3 β were analyzed by western blotting in HepG2 and Huh7 cells after treatment with E3330 (50 μ M) for 24 h. **K, L** Protein levels of APE1, NRF2, p-GSK3 β , and GSK3 β in HepG2 and Huh7 cells after overexpression of APE1-WT and APE1-C65A were analyzed by western blotting. Data are shown as the mean \pm SD ($n = 3$). * $P < 0.05$, ** $P < 0.01$.

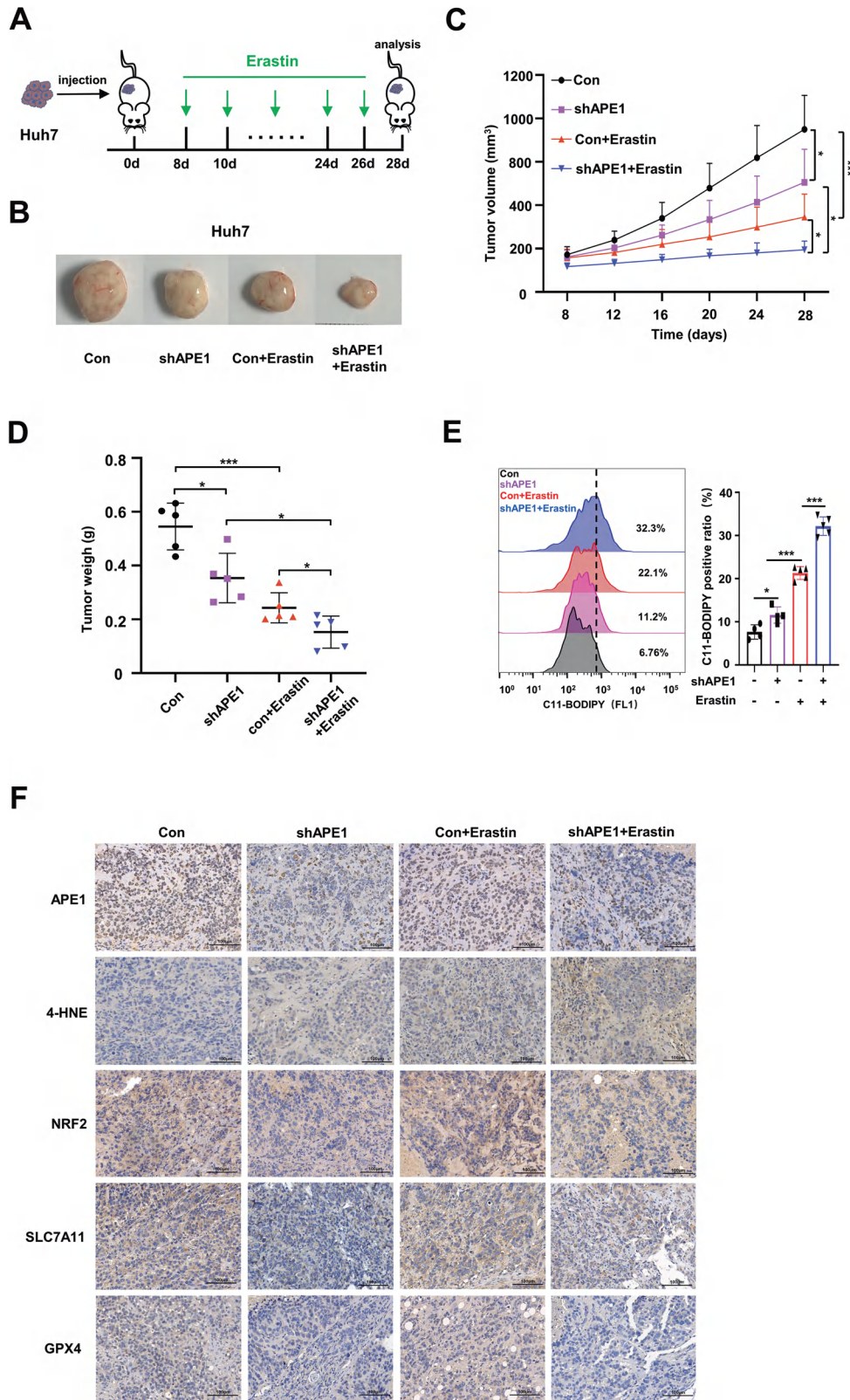


Fig. 7 APE1 inhibition enhances the sensitivity of HCC to ferroptosis in vivo. **A** Schematic description of the animal experimental design. **B** Representative images of dissected xenografts from the indicated groups at the end of the experiments. **C** The volume of Huh7 xenografts treated with erastin at different time points. Error bars are presented as mean \pm SD from 5 independent repeats. *P* values were calculated using two-tailed unpaired Student's *t* test. **D** The weight of the xenograft tumor at the end of the experiment. Error bars are presented as mean \pm SD from 5 independent repeats. *P* values were calculated using two-tailed unpaired Student's *t* test. **E** Lipid peroxidation levels in the tumor were detected using C11-BODIPY staining. **F** The expressions of APE1, 4-HNE, NRF2, SLC7A11, and GPX4 were determined by immunohistochemical staining. **P* < 0.05, ****P* < 0.001.

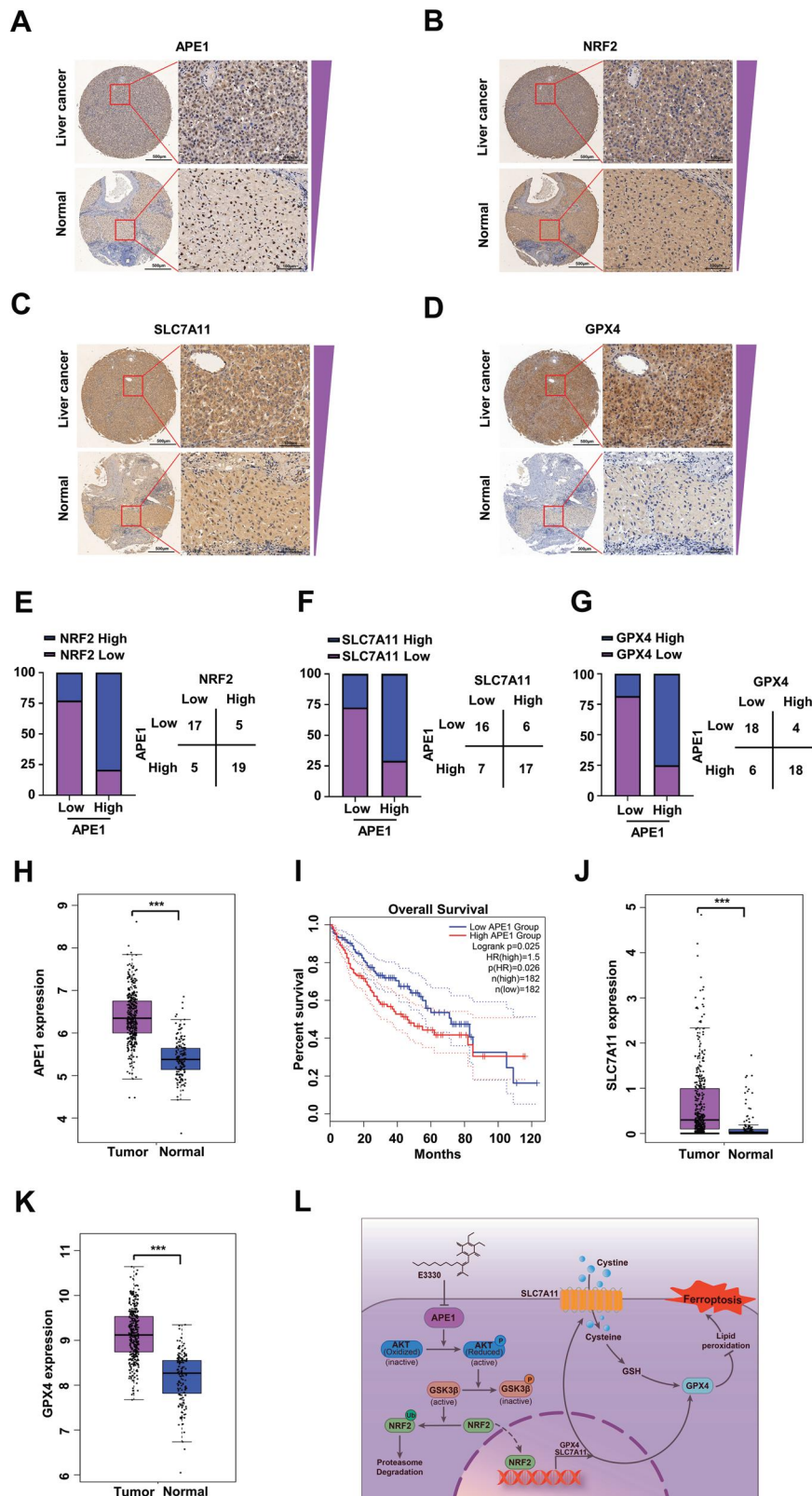


Fig. 8 APE1-mediated expression of SLC7A11 and GPX4 via NRF2 is clinically associated with the progression and prognosis of HCC. **A–D** Tissue microarray of APE1, NRF2, SLC7A11, and GPX4 in liver cancer and normal liver tissues, as measured by IHC. **E–G** The correlation of APE1 with NRF2, SLC7A11, and GPX4 was analyzed on 46 HCC tissue microarrays. **H** Statistical analysis of APE1 mRNA expression levels in Liver hepatocellular carcinoma (LIHC) from the TCGA database. **I** Kaplan–Meier survival analysis for clinical LIHC patients with APE1 expression in tumor tissues from the TCGA database. **J** Statistical analysis of SLC7A11 mRNA expression levels in LIHC from the TCGA database. **K** Statistical analysis of GPX4 mRNA expression levels in LIHC from the TCGA database. **L** The schematic representation of APE1 inhibition enhancing ferroptosis in hepatocellular carcinoma cells. *** $P < 0.001$.

studies have found that components of the DNA damage repair pathway are capable of regulating ferroptosis, most of which are involved through non-canonical mechanisms. For example, p53 regulates ferroptosis by affecting multiple mechanisms, such as modulating the expression of SLC7A11 and ACSL4 and promoting the translocation of DPP4 [57]. Most of these target genes regulating ferroptosis are not directly involved in the canonical phenotypic effects of DDR (proliferation arrest, DNA repair, or apoptosis). We further explored the relationship between the redox function of APE1 and ferroptosis. We found that the use of E3330, a specific inhibitor of APE1 redox function, promoted erastin- and RSL3-induced ferroptosis. Moreover, treatment of cells with E3330 decreased the protein level of NRF2 and suppressed the expression of SLC7A11 and GPX4. Interestingly, short-term treatment of cells with E3330 increased the protein level of NRF2. The increase in NRF2 protein levels may be due to the treatment of cells with E3330, which induces oxidative stress and upregulates expression of NRF2 in order to protect the cells in response to oxidative stress. However, with the duration of APE1 inhibition increased, the cells exhibited increased GSK3 β activity, resulting in reduced degradation of NRF2 protein through the ubiquitin/proteasome pathway. In addition, we constructed mutant forms of APE1, including a DNA damage repair function-deficient mutant (H309N) and a redox function-deficient mutant (C65A), to further demonstrate the involvement of APE1 in ferroptosis in HCC specifically through its redox function.

Overall, our study suggests that APE1 inhibition promotes ferroptosis in HCC cells. The deletion or inhibition of APE1's redox function increases AKT in the oxidized state, inhibiting its phosphorylation and activation, allowing downstream GSK3 β to be activated via dephosphorylation, which leads to the degradation of NRF2 via the ubiquitin/proteasome pathway. Then downregulation of NRF2 repressed the expression of SLC7A11 and GPX4, triggering ferroptosis in HCC cells and contributing to ferroptosis-based HCC therapy. These findings highlight the potential of targeting APE1 to enhance ferroptosis as a promising strategy for HCC therapy. APE1 inhibitors could serve as potential therapeutic targets for HCC patients, offering new insights and potential approaches for the treatment of this disease.

DATA AVAILABILITY

All data needed to evaluate the conclusions in the paper are present in the paper. Additional data related to this paper may be requested from the corresponding author.

REFERENCES

- Favre S, Rimassa L, Finn RS. Molecular therapies for HCC: Looking outside the box. *J Hepatol*. 2020;72:342–52.
- Dixon SJ, Lemberg KM, Lamprecht MR, Skouta R, Zaitsev EM, Gleason CE, et al. Ferroptosis: an iron-dependent form of nonapoptotic cell death. *Cell*. 2012;149:1060–72.
- Jiang L, Kon N, Li T, Wang SJ, Su T, Hibshoosh H, et al. Ferroptosis as a p53-mediated activity during tumour suppression. *Nature*. 2015;520:57–62.
- Wang W, Green M, Choi JE, Gijon M, Kennedy PD, Johnson JK, et al. CD8(+) T cells regulate tumour ferroptosis during cancer immunotherapy. *Nature*. 2019;569:270–4.
- Lang X, Green MD, Wang W, Yu J, Choi JE, Jiang L, et al. Radiotherapy and Immunotherapy Promote Tumoral Lipid Oxidation and Ferroptosis via Synergistic Repression of SLC7A11. *Cancer Discov*. 2019;9:1673–85.
- Kagan VE, Mao G, Qu F, Angeli JP, Doll S, Croix CS, et al. Oxidized arachidonic and adrenic PEs navigate cells to ferroptosis. *Nat Chem Biol*. 2017;13:81–90.
- Koppula P, Zhuang L, Gan B. Cystine transporter SLC7A11/xCT in cancer: ferroptosis, nutrient dependency, and cancer therapy. *Protein Cell*. 2021;12:599–620.
- Yang WS, SriRamaratnam R, Welsch ME, Shimada K, Skouta R, Viswanathan VS, et al. Regulation of ferroptotic cancer cell death by GPX4. *Cell*. 2014;156:317–31.
- Chen J, Li X, Ge C, Min J, Wang F. The multifaceted role of ferroptosis in liver disease. *Cell Death Differ*. 2022;29:467–80.
- Liao H, Shi J, Wen K, Lin J, Liu Q, Shi B, et al. Molecular Targets of Ferroptosis in Hepatocellular Carcinoma. *J Hepatocell Carcinoma*. 2021;8:985–96.
- Chen Q, Zheng W, Guan J, Liu H, Dan Y, Zhu L, et al. SOCS2-enhanced ubiquitination of SLC7A11 promotes ferroptosis and radiosensitization in hepatocellular carcinoma. *Cell Death Differ*. 2023;30:137–51.
- Wang Q, Bin C, Xue Q, Gao Q, Huang A, Wang K, et al. GSTZ1 sensitizes hepatocellular carcinoma cells to sorafenib-induced ferroptosis via inhibition of NRF2/GPX4 axis. *Cell Death Dis*. 2021;12:426.
- Bhakat KK, Mantha AK, Mitra S. Transcriptional regulatory functions of mammalian AP-endonuclease (APE1/Ref-1), an essential multifunctional protein. *Antioxid Redox Signal*. 2009;11:621–38.
- Demple B, Herman T, Chen DS. Cloning and expression of APE, the cDNA encoding the major human apurinic endonuclease: definition of a family of DNA repair enzymes. *Proc Natl Acad Sci USA*. 1991;88:11450–4.
- Li M, Wilson DM 3rd. Human apurinic/aprimidinic endonuclease 1. *Antioxid Redox Signal*. 2014;20:678–707.
- Kelley MR, Georgiadis MM, Fishel ML. APE1/Ref-1 role in redox signaling: translational applications of targeting the redox function of the DNA repair/redox protein APE1/Ref-1. *Curr Mol Pharm*. 2012;5:36–53.
- Nishi T, Shimizu N, Hiramoto M, Sato I, Yamaguchi Y, Hasegawa M, et al. Spatial redox regulation of a critical cysteine residue of NF-kappa B in vivo. *J Biol Chem*. 2002;277:44548–56.
- Logsdon DP, Grimard M, Luo M, Shahda S, Jiang Y, Tong Y, et al. Regulation of HIF1alpha under Hypoxia by APE1/Ref-1 Impacts CA9 Expression: Dual Targeting in Patient-Derived 3D Pancreatic Cancer Models. *Mol Cancer Ther*. 2016;15:2722–32.
- Ando K, Hirao S, Kabe Y, Ogura Y, Sato I, Yamaguchi Y, et al. A new APE1/Ref-1-dependent pathway leading to reduction of NF-kappaB and AP-1, and activation of their DNA-binding activity. *Nucleic Acids Res*. 2008;36:4327–36.
- Seo YR, Kelley MR, Smith ML. Selenomethionine regulation of p53 by a ref1-dependent redox mechanism. *Proc Natl Acad Sci USA*. 2002;99:14548–53.
- Caston RA, Gampala S, Armstrong L, Messmann RA, Fishel ML, Kelley MR. The multifunctional APE1 DNA repair-redox signaling protein as a drug target in human disease. *Drug Discov Today*. 2021;26:218–28.
- Lu X, Zhao H, Yuan H, Chu Y, Zhu X. High nuclear expression of APE1 correlates with unfavorable prognosis and promotes tumor growth in hepatocellular carcinoma. *J Mol Histol*. 2021;52:219–31.
- Li E, Xia M, Du Y, Long K, Ji F, Pan F, et al. METTL3 promotes homologous recombination repair and modulates chemotherapeutic response in breast cancer by regulating the EGF/RAD51 axis. *Elife*. 2022;11:e75231.
- Yang F, Hu Z, Guo Z. Small-Molecule Inhibitors Targeting FEN1 for Cancer Therapy. *Biomolecules*. 2022;12:1007.
- Ji F, Zhang F, Zhang M, Long K, Xia M, Lu F, et al. Targeting the DNA damage response enhances CD70 CAR-T cell therapy for renal carcinoma by activating the cGAS-STING pathway. *J Hematol Oncol*. 2021;14:152.
- Long K, Gu L, Li L, Zhang Z, Li E, Zhang Y, et al. Small-molecule inhibition of APE1 induces apoptosis, pyroptosis, and necroptosis in non-small cell lung cancer. *Cell Death Dis*. 2021;12:503.
- Zhao H, Ding Y, Zhang L. SIRT1/APE1 promotes the viability of gastric cancer cells by inhibiting p53 to suppress ferroptosis. *Open Med (Wars)*. 2023;18:20220620.
- Yue R, Zhou M, Li X, Xu L, Lu C, Dong Z, et al. GSH/APE1 Cascade-Activated NanoplatforM for Imaging Therapy Resistance Dynamics and Enzyme-Mediated Adaptive Ferroptosis. *ACS Nano*. 2023;17:13792–810.
- Kobayashi T, Kishigami S, Sone M, Inokuchi H, Mogi T, Ito K. Respiratory chain is required to maintain oxidized states of the DsbA-DsbB disulfide bond formation system in aerobically growing *Escherichia coli* cells. *Proc Natl Acad Sci USA*. 1997;94:11857–62.
- Sriramajayam K, Peng D, Lu H, Zhou S, Bhat N, McDonald OG, et al. Activation of NRF2 by APE1/REF1 is redox-dependent in Barrett's related esophageal adenocarcinoma cells. *Redox Biol*. 2021;43:101970.
- Tang D, Chen X, Kang R, Kroemer G. Ferroptosis: molecular mechanisms and health implications. *Cell Res*. 2021;31:107–25.
- Habib E, Linher-Melville K, Lin HX, Singh G. Expression of xCT and activity of system xc(-) are regulated by NRF2 in human breast cancer cells in response to oxidative stress. *Redox Biol*. 2015;5:33–42.
- Yuan S, Wei C, Liu G, Zhang L, Li J, Li L, et al. Sorafenib attenuates liver fibrosis by triggering hepatic stellate cell ferroptosis via HIF-1alpha/SLC7A11 pathway. *Cell Prolif*. 2022;55:e13158.
- Feng H, Liu Y, Gan Y, Li M, Liu R, Liang Z, et al. AdipoR1 Regulates Ionizing Radiation-Induced Ferroptosis in HCC cells through Nrf2/xCT Pathway. *Oxid Med Cell Longev*. 2022;2022:8091464.
- Hayes JD, Dinkova-Kostova AT. The Nrf2 regulatory network provides an interface between redox and intermediary metabolism. *Trends Biochem Sci*. 2014;39:199–218.
- Rada P, Rojo AI, Evrard-Todeschi N, Innamorato NG, Cotte A, Jaworski T, et al. Structural and functional characterization of Nrf2 degradation by the glycogen synthase kinase 3/beta-TrCP axis. *Mol Cell Biol*. 2012;32:3486–99.

37. Sharma M, Chuang WW, Sun Z. Phosphatidylinositol 3-kinase/Akt stimulates androgen pathway through GSK3 β inhibition and nuclear beta-catenin accumulation. *J Biol Chem*. 2002;277:30935–41.
38. Murata H, Ihara Y, Nakamura H, Yodoi J, Sumikawa K, Kondo T. Glutaredoxin exerts an antiapoptotic effect by regulating the redox state of Akt. *J Biol Chem*. 2003;278:50226–33.
39. Yao F, Deng Y, Zhao Y, Mei Y, Zhang Y, Liu X, et al. A targetable LIFR-NF- κ B-LCN2 axis controls liver tumorigenesis and vulnerability to ferroptosis. *Nat Commun*. 2021;12:7333.
40. Gao R, Kalathur RKR, Coto-Llerena M, Ercan C, Buechel D, Shuang S, et al. YAP/TAZ and ATF4 drive resistance to Sorafenib in hepatocellular carcinoma by preventing ferroptosis. *EMBO Mol Med*. 2021;13:e14351.
41. Lei G, Zhang Y, Koppula P, Liu X, Zhang J, Lin SH, et al. The role of ferroptosis in ionizing radiation-induced cell death and tumor suppression. *Cell Res*. 2020;30:146–62.
42. Viswanathan VS, Ryan MJ, Dhruv HD, Gill S, Eichhoff OM, Seashore-Ludlow B, et al. Dependency of a therapy-resistant state of cancer cells on a lipid peroxidase pathway. *Nature*. 2017;547:453–7.
43. Wu J, Minikes AM, Gao M, Bian H, Li Y, Stockwell BR, et al. Intercellular interaction dictates cancer cell ferroptosis via NF2-YAP signalling. *Nature*. 2019;572:402–6.
44. Gao M, Yi J, Zhu J, Minikes AM, Monian P, Thompson CB, et al. Role of Mitochondria in Ferroptosis. *Mol Cell*. 2019;73:354–63.e353.
45. Ma X, Dang C, Min W, Diao Y, Hui W, Wang X, et al. Downregulation of APE1 potentiates breast cancer cells to olaparib by inhibiting PARP-1 expression. *Breast Cancer Res Treat*. 2019;176:109–17.
46. Bersuker K, Hendricks JM, Li Z, Magtanong L, Ford B, Tang PH, et al. The CoQ oxidoreductase FSP1 acts parallel to GPX4 to inhibit ferroptosis. *Nature*. 2019;575:688–92.
47. Doll S, Proneth B, Tyurina YY, Panzilius E, Kobayashi S, Ingold I, et al. ACSL4 dictates ferroptosis sensitivity by shaping cellular lipid composition. *Nat Chem Biol*. 2017;13:91–8.
48. Liu J, Ren Z, Yang L, Zhu L, Li Y, Bie C, et al. The NSUN5-FTH1/FTL pathway mediates ferroptosis in bone marrow-derived mesenchymal stem cells. *Cell Death Discov*. 2022;8:99.
49. Dodson M, Castro-Portuguez R, Zhang DD. NRF2 plays a critical role in mitigating lipid peroxidation and ferroptosis. *Redox Biol*. 2019;23:101107.
50. Cuadrado A. Structural and functional characterization of Nrf2 degradation by glycogen synthase kinase 3/ β -TrCP. *Free Radic Biol Med*. 2015;88:147–57.
51. Park MS, Kim CS, Joo HK, Lee YR, Kang G, Kim SJ, et al. Cytoplasmic localization and redox cysteine residue of APE1/Ref-1 are associated with its anti-inflammatory activity in cultured endothelial cells. *Mol Cells*. 2013;36:439–45.
52. Di Maso V, Avellini C, Croce LS, Rosso N, Quadrioglio F, Cesaratto L, et al. Subcellular localization of APE1/Ref-1 in human hepatocellular carcinoma: possible prognostic significance. *Mol Med*. 2007;13:89–96.
53. Lu GS, Li M, Xu CX, Wang D. APE1 stimulates EGFR-TKI resistance by activating Akt signaling through a redox-dependent mechanism in lung adenocarcinoma. *Cell Death Dis*. 2018;9:1111.
54. Whitaker AM, Freudenthal BD. APE1: A skilled nucleic acid surgeon. *DNA Repair*. 2018;71:93–100.
55. Li M, Yang X, Lu X, Dai N, Zhang S, Cheng Y, et al. APE1 deficiency promotes cellular senescence and premature aging features. *Nucleic Acids Res*. 2018;46:5664–77.
56. Liu J, Kang R, Tang D. Signaling pathways and defense mechanisms of ferroptosis. *FEBS J*. 2022;289:7038–50.
57. Chen PH, Tseng WH, Chi JT. The Intersection of DNA Damage Response and Ferroptosis-A Rationale for Combination Therapeutics. *Biology*. 2020;9:187.

AUTHOR CONTRIBUTIONS

Y.D., Y.Z., and X.Y. performed study concept and design; Z.H., Y.D., Z.G., L.H. and F.P. performed development of methodology and writing, review and revision of the paper; Y.D., Y.Z., X.Y., Z.H. and Z.G. provided acquisition, analysis and interpretation of data, and statistical analysis; F.P., Z.H., L.H. and Z.G. provided technical and material support. All authors read and approved the final paper.

FUNDING

This work was supported by the National Natural Science Foundation of China (32171407 and 82373183) and the Priority Academic Program Development of Jiangsu Higher Education Institutions.

COMPETING INTERESTS

The authors declare no competing interests.

ETHICS APPROVAL

This research was approved by the Ethics Committee of Nanjing Normal University. All animal experiments were performed according to procedures approved by the Laboratory Animal Care Committee at Nanjing Normal University, in accordance with the National Institutes of Health Guide for the Care and Use of Laboratory Animals.

ADDITIONAL INFORMATION

Supplementary information The online version contains supplementary material available at <https://doi.org/10.1038/s41418-024-01270-0>.

Correspondence and requests for materials should be addressed to Zhigang Guo or Zhigang Hu.

Reprints and permission information is available at <http://www.nature.com/reprints>

Publisher's note Springer Nature remains neutral with regard to jurisdictional claims in published maps and institutional affiliations.

Springer Nature or its licensor (e.g. a society or other partner) holds exclusive rights to this article under a publishing agreement with the author(s) or other rightsholder(s); author self-archiving of the accepted manuscript version of this article is solely governed by the terms of such publishing agreement and applicable law.